

# Tentative detection of $\text{HC}_5\text{NH}^+$ in TMC-1<sup>★</sup>

N. Marcelino<sup>1</sup>, M. Agúndez<sup>1</sup>, B. Tercero<sup>2,3</sup>, C. Cabezas<sup>1</sup>, C. Bermúdez<sup>1</sup>, J. D. Gallego<sup>2</sup>, P. de Vicente<sup>2</sup>, J. Cernicharo<sup>1</sup>

<sup>1</sup> Grupo de Astrofísica Molecular, Instituto de Física Fundamental (IFF-CSIC), C/ Serrano 121, 28006 Madrid, Spain. e-mail: : jose.cernicharo@csic.es

<sup>2</sup> Centro de Desarrollos Tecnológicos, Observatorio de Yebes (IGN), 19141 Yebes, Guadalajara, Spain.

<sup>3</sup> Observatorio Astronómico Nacional (IGN), C/ Alfonso XII, 3, 28014, Madrid, Spain.

Received; accepted

## ABSTRACT

Using the Yebes 40m radio telescope, we report the detection of a series of seven lines harmonically related with a rotational constant  $B_0=1295.81581 \pm 0.00026$  MHz and a distortion constant  $D_0=27.3 \pm 0.5$  Hz towards the cold dense cloud TMC-1. Ab initio calculations indicate that the best possible candidates are the cations  $\text{HC}_5\text{NH}^+$  and  $\text{NC}_4\text{NH}^+$ . From a comparison between calculated and observed rotational constants and other arguments based on proton affinities and dipole moments, we conclude that the best candidate for a carrier of the observed lines is the protonated cyanodiacetylene cation,  $\text{HC}_5\text{NH}^+$ . The  $\text{HC}_5\text{N}/\text{HC}_5\text{NH}^+$  ratio derived in TMC-1 is 240, which is very similar to the  $\text{HC}_3\text{N}/\text{HC}_3\text{NH}^+$  ratio. Results are discussed in the framework of a chemical model for protonated molecules in cold dense clouds.

**Key words.** Astrochemistry — ISM: molecules — ISM: individual (TMC-1) — line: identification — molecular data

## 1. Introduction

Although gas phase chemistry in cold interstellar clouds is dominated by ion-neutral reactions, only around 15% of the detected species are cations (see the Cologne Database for Molecular Spectroscopy; Müller et al. 2005). Observed polyatomic cations are usually protonated forms of stable molecules. The rather reduced number of them detected in space is due to the fact that a dissociative recombination with electrons is rapid and depletes cations, producing most of the neutrals observed in these objects. In addition to the widespread ions  $\text{HCO}^+$  and  $\text{N}_2\text{H}^+$ , other interesting protonated species are  $\text{HCS}^+$  (Thaddeus et al. 1981),  $\text{HCNH}^+$  (Schilke et al. 1991),  $\text{HC}_3\text{NH}^+$  (Kawaguchi et al. 1994),  $\text{HCO}_2^+$  (Turner et al. 1999; Sakai et al. 2008),  $\text{NH}_3\text{D}^+$  (Cernicharo et al. 2013),  $\text{NCCNH}^+$  (Agúndez et al. 2015),  $\text{H}_2\text{COH}^+$  (Bacmann et al. 2016), and  $\text{H}_2\text{NCO}^+$  (Marcelino et al. 2018).

The abundance ratio between a protonated molecule and its neutral counterpart,  $[\text{MH}^+]/[\text{M}]$ , is sensitive to the degree of ionisation and to the proton affinity of the neutral. The higher the density is, the lower the ionisation fraction is and thus the lower the importance of protonated molecules. It is interesting to note that both the chemical models and the observations suggest a trend in which the abundance ratio  $[\text{MH}^+]/[\text{M}]$  increases with an increasing proton affinity of M (Agúndez et al. 2015).

Protonated nitriles and dinitriles are observed in cold dense clouds because their neutral counterparts are abundant and have high proton affinities. The nitriles HCN and  $\text{HC}_3\text{N}$  have proton affinities of  $712.9 \text{ kJ mol}^{-1}$  and  $751.2 \text{ kJ mol}^{-1}$ , respectively (Hunter & Lias 1998), and abundances in excess of  $10^{-8}$  relative to  $\text{H}_2$  (Agúndez & Wakelam 2013). Whereas the dinitrile NCCN has a proton affinity of  $674.7 \text{ kJ mol}^{-1}$  (Hunter & Lias 1998)

and an inferred abundance as large as that of HCN and  $\text{HC}_3\text{N}$  (Agúndez et al. 2015, 2018). The next larger members in the series of cyanopolyynes and dicyanopolyynes are also good candidates to be detected in their protonated form. Cyanodiacetylene ( $\text{HC}_5\text{N}$ ) has a high proton affinity ( $770 \pm 20 \text{ kJ mol}^{-1}$ ; Edwards et al. 2009) and it is just a few times less abundant than  $\text{HC}_3\text{N}$  in cold dark cores (Agúndez & Wakelam 2013). Dicyanoacetylene ( $\text{NC}_4\text{N}$ ) also has a high proton affinity ( $736 \text{ kJ mol}^{-1}$ ; this work) and it is likely to be present with a high abundance based on the large inferred abundance of NCCN. Hence, we could expect the protonated forms of  $\text{HC}_5\text{N}$  and  $\text{NC}_4\text{N}$  to be present in cold dense clouds with moderately high abundances.

In this Letter, we report the detection of a new series of harmonically related lines belonging to a molecule with a  $^1\Sigma$  ground electronic state towards the cold dark core TMC-1. Two of the molecular species discussed above,  $\text{HC}_5\text{NH}^+$  and  $\text{NC}_4\text{NH}^+$ , could be the carriers. From ab initio calculations and the expected intensities of the lines for each of these species, we conclude that we have discovered the cation  $\text{HC}_5\text{NH}^+$ . No laboratory data are available for it, hence, this is the first time this species has been observed. Abundance ratios between  $\text{HC}_3\text{N}$  and  $\text{HC}_5\text{N}$  and their protonated forms were derived and compared with predictions from chemical models. We searched for lines that could be attributed to  $\text{NC}_4\text{NH}^+$  without success. A search for  $\text{NC}_3\text{NC}$  in our data also provides upper limits to the abundance of this species.

## 2. Observations

New receivers, which were built within the Nanocosmos project<sup>1</sup> and installed at the Yebes 40m radio telescope, were used for the observations of TMC-1. The Q-band receiver consists of two HEMT cold amplifiers covering the 31.0-50.3 GHz band with

<sup>★</sup> Based on observations carried out with the Yebes 40m telescope (projects 19A003 and 20A014). The 40m radiotelescope at Yebes Observatory is operated by the Spanish Geographic Institute (IGN, Ministerio de Transportes, Movilidad y Agenda Urbana).

<sup>1</sup> <https://nanocosmos.iff.csic.es/>

**Table 1.** Observed line parameters for the new molecule in TMC-1.

$J_u$	$\nu_{obs}^a$ (MHz)	$\nu_o - \nu_c^b$ (kHz)	$\Delta\nu^c$ (kms $^{-1}$ )	$\int T_A^* dv^d$ (mK kms $^{-1}$ )	$T_A^*$ (mK)
13	33690.975	+5.2	0.80±0.05	8.2±1.0	9.7
14	36282.540	-2.6	0.73±0.04	8.0±1.0	10.4
15	38874.102	-3.3	0.59±0.05	5.9±1.0	9.4
16	41465.655	-3.1	0.46±0.05	4.5±1.0	11.9
17	44057.202	+1.7	0.76±0.09	5.1±1.0	6.3
18	46648.736	+4.5	0.68±0.08	5.3±1.0	7.7
19	49240.242	-8.8	0.50±0.10	2.7±1.0	5.0

**Notes.**

<sup>(a)</sup> Observed frequencies for a  $v_{LSR}$  of 5.83 km s $^{-1}$ . The uncertainty is 10 kHz for all lines, except for  $J=19-18$  for which it is 20 kHz.

<sup>(b)</sup> Observed minus calculated frequencies in kHz.

<sup>(c)</sup> Linewidth at half intensity derived by fitting a Gaussian line profile to the observed transitions (in kms $^{-1}$ ).

<sup>(d)</sup> Integrated line intensity in mK kms $^{-1}$

horizontal and vertical polarisations. Receiver temperatures vary from 22 K at 32 GHz to 42 K at 50 GHz. The spectrometers are  $2 \times 8 \times 2.5$  GHz FFTs with a spectral resolution of 38.1 kHz, providing the whole coverage of the Q-band in both polarisations. The main beam efficiency and the half power beam width (HPBW) of the Yebes 40 m telescope range from 0.6 and 55'' (at 32 GHz) to 0.43 and 37'' (at 49 GHz), respectively.

The observations leading to the line survey in the Q-band towards TMC-1 ( $\alpha_{J2000} = 4^h41^m41.9^s$ ,  $\delta_{J2000} = +25^\circ41'27.0''$ ) were performed during several sessions between November 2019 and February 2020. The observing procedure used was frequency switching with a frequency throw of 10 MHz. The nominal spectral resolution of 38.1 kHz was used for the final spectra. A study of the velocity structure of the source (see, e.g. Lique et al. 2006; Xue et al. 2020) could require a higher spectral resolution. However, the determination of the total column density in the line of sight for a given molecule is not affected by our spectral resolution of 38.1 kHz. The sensitivity varies along the Q-band between 1 and 3 mK, which considerably improves previous line surveys in the 31-50 GHz frequency range (Kaifu et al. 2004).

The intensity scale, antenna temperature ( $T_A^*$ ) was calibrated using two absorbers at different temperatures and the atmospheric transmission model (ATM, Cernicharo 1985; Pardo et al. 2001). Calibration uncertainties have been adopted to be 10 %. All data have been analysed using the GILDAS package<sup>2</sup>.

### 3. Results

One of the most surprising results from the line survey in the Q-band in TMC-1 is the presence of a forest of weak lines. Most of them can be assigned to known species and their isotopologues, and only a few remain unidentified (Marcelino et al., in preparation). As previously mentioned, the level of sensitivity has been increased by a factor of 5-10 with respect to previous line surveys performed with other telescopes at these frequencies (Kaifu et al. 2004). Frequencies for the unknown lines have been derived by assuming a local standard of rest velocity of 5.83 km s $^{-1}$ , which is a value that was derived from the observed transitions of HC<sub>5</sub>N and its isotopologues in our line survey.

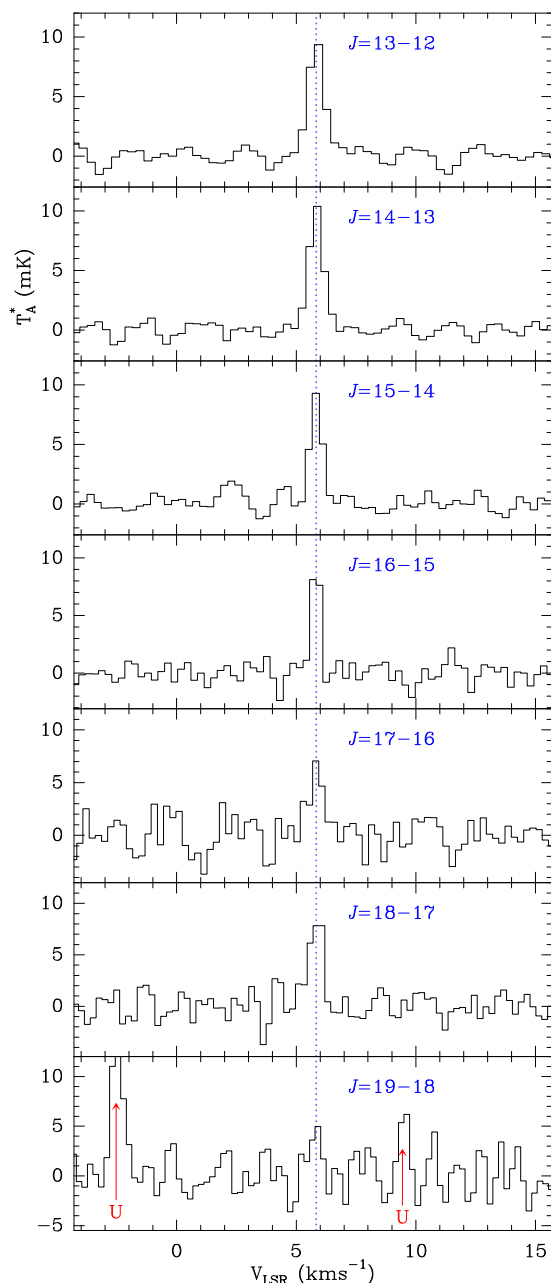


**Fig. 1.** Observed lines of the new molecule found in the 31-50 GHz domain towards TMC-1. The abscissa corresponds to the local standard of rest velocity in km s $^{-1}$ . Frequencies and intensities for the observed lines are given in Table 1. The ordinate is the antenna temperature corrected for atmospheric and telescope losses in mK. The  $J=19-18$  line is only detected at a  $3.5\sigma$  level. Spectral resolution is 38.1 kHz.

#### 3.1. Harmonically related lines

Among the unidentified features in our survey, we have found a series of seven harmonically related lines to a precision better than  $2 \times 10^{-7}$ . This strongly suggests that the carrier is a linear molecule with a  $^1\Sigma$  ground electronic state. Fig. 1 shows these lines and the quantum numbers that were obtained. The derived line parameters are given in Table 1. Using the MADEx code (Cernicharo 2012), we have verified that none of these features can be assigned to lines from other species. For a linear molecule, the frequencies of its rotational transitions follow the standard expression  $\nu(J \rightarrow J-1) = 2B_0J - 4D_0J^3$ . By fitting the

<sup>2</sup> <http://www.iram.fr/IRAMFR/GILDAS>

frequencies of the lines given in Table 1, we derive

$$B_0 = 1295.81581(26) \text{ MHz}$$

$$D_0 = 27.4(5) \times 10^{-6} \text{ MHz},$$

where values between parentheses represent the  $1\sigma$  uncertainty on the parameters in units of the last digit. The standard deviation of the fit is 5.6 kHz.

The rotation constant is  $\sim 36$  MHz lower than that of HC<sub>5</sub>N (1331.332 MHz; Bizzocchi et al. 2004). It is also lower than that of dicyanoacetylene, NCCCCN (1336.7 MHz; Winther et al. 1992). The rotational constants of the <sup>13</sup>C and <sup>15</sup>N isotopologues of HC<sub>5</sub>N are well known from laboratory measurements (Bizzocchi et al. 2004; Giesen et al. 2020). The isotopologues HC<sub>5</sub><sup>15</sup>N and H<sup>13</sup>CCCCCN have rotational constants of 1298.640 MHz and 1296.676 MHz, respectively, that is to say they are very close to that of the new species, suggesting that a slightly heavier species could be the carrier. The isomer HC<sub>4</sub>NC has a larger rotational constant of 1401.182 MHz (Botschwina et al. 1998) and it can be excluded as a carrier. Moreover, this species has been detected in our line survey (Cernicharo et al. 2020) and also by Xue et al. (2020). Although the isomer HNC<sub>5</sub> has not been observed in the laboratory, ab initio calculations indicate that the molecule is bent with a  $(B + C)/2$  value of  $\sim 1363$  MHz (Gronowski & Kolos 2006; Cernicharo et al. 2020), which is  $\sim 70$  MHz above the observed rotational constant.

In TMC-1, only polyatomic molecules containing H, C, N, O, and S have been found so far. We could consider a linear chain containing sulphur as a possible carrier. However, the best candidate in this case is HC<sub>4</sub>S, which is linear but has a <sup>2</sup>Π<sub>i</sub> ground electronic state and a rotational constant of 1435.326 MHz that is too high (Hirahara et al. 1994). Another potential species is NCCCS, which is linear, but also with a <sup>2</sup>Π<sub>i</sub> ground electronic state and a rotational constant of 1439.186 MHz (McCarthy et al. 2003). The neutral species HC<sub>5</sub>O was observed in the laboratory by Mohamed et al. (2005). It has a rotational constant of 1293.6 MHz and has been observed in TMC-1 (McGuire et al. 2017). Hence, good candidates for the carrier of the observed lines are molecular species having a structure and mass close to that of HC<sub>5</sub>N, HC<sub>5</sub>O, or NC<sub>4</sub>N.

The cation HC<sub>3</sub>NH<sup>+</sup> was detected towards TMC-1 by Kawaguchi et al. (1994); additionally, protonated cyanogen, HNCCN<sup>+</sup>, was also detected in this source by Agúndez et al. (2015). Hence, good candidates for the carrier of the series of harmonically related lines are HC<sub>5</sub>NH<sup>+</sup> and NC<sub>4</sub>NH<sup>+</sup>. An additional candidate is HC<sub>5</sub>O<sup>+</sup>, which could be the product of protonation of C<sub>5</sub>O. However, C<sub>5</sub>O has not been detected so far in space and ab initio calculations (see below) indicate a rotational constant several MHz above the observed one. For protonated cyanodiacetylene, HC<sub>5</sub>NH<sup>+</sup>, ab initio calculations by Botschwina et al. (1997) indicate an equilibrium rotational constant very close to ours of  $\sim 1294.1$  MHz with a dipole moment of 3.811 D. It is a very good candidate indeed as the difference between the predicted and the observed rotational constant is less than 0.1%. Nevertheless, since we have a good second candidate, NC<sub>4</sub>NH<sup>+</sup>, and also a third (less clear) possibility, HC<sub>5</sub>O<sup>+</sup>, additional calculations are needed to help with the assignment of the lines.

### 3.2. Quantum chemical calculations

As mentioned before, HC<sub>5</sub>NH<sup>+</sup>, NC<sub>4</sub>NH<sup>+</sup>, and HC<sub>5</sub>O<sup>+</sup> are the three candidates that have a rotational constant compatible with that derived from the lines observed in TMC-1. In order to obtain

**Table 2.** Rotational constants and electric dipole moments calculated for HC<sub>5</sub>NH<sup>+</sup> and NC<sub>4</sub>NH<sup>+</sup>.

Parameter	New molecule <sup>a</sup>	HC <sub>5</sub> NH <sup>+</sup>	NC <sub>4</sub> NH <sup>+</sup>	HC <sub>5</sub> O <sup>+</sup>
$B_0$ (MHz)	1295.8158(3)	1295.51	1293.54	1303.12
$D_e$ (MHz)	$27.4(5) \times 10^{-6}$	$26.3 \times 10^{-6}$	$27.8 \times 10^{-6}$	$31.2 \times 10^{-6}$
$\mu$ (D)		3.26	9.47	3.10

#### Notes.

<sup>(a)</sup> Values derived from the frequencies observed in TMC-1 (see Section 3.1). Values between parentheses represent the  $1\sigma$  uncertainty in units of the last digit.

precise geometries and spectroscopic molecular parameters that help with the assignment of the observed lines, we carried out high-level ab initio calculations for these three species. Other structural isomers of HC<sub>5</sub>NH<sup>+</sup> and NC<sub>4</sub>NH<sup>+</sup> species were discarded as candidates because of their rotational constant values and their energetics; all metastable isomers lie at least at 18 kcal mol<sup>-1</sup> over the HC<sub>5</sub>NH<sup>+</sup> and NC<sub>4</sub>NH<sup>+</sup> species, see Table B.3. Therefore, the calculations presented below are restricted to HC<sub>5</sub>NH<sup>+</sup>, NC<sub>4</sub>NH<sup>+</sup>, and HC<sub>5</sub>O<sup>+</sup> molecules. Details regarding the calculations can be found in Appendix B.

The experimental rotational parameters for HC<sub>5</sub>N, NC<sub>4</sub>N, and C<sub>5</sub>O have been determined before (Bizzocchi et al. 2004; Winther et al. 1992; Ogata et al. 1995) and, therefore, they can be used to calibrate the computational results of their corresponding protonated forms. The  $B_e$  rotational constant for HC<sub>5</sub>N, NC<sub>4</sub>N, and C<sub>5</sub>O, which were calculated at the CCSD(T)-F12/cc-pCVTZ-F12 level of theory, are 1329.57, 1334.69, and 1363.74 MHz, respectively. The zero-point vibrational contributions to the rotational constant at the MP2/cc-pVTZ level of theory were calculated to be 0.62, 0.72, and 1.82 MHz, respectively. Adding this contribution to the above  $B_e$ ,  $B_0$  thus takes values of 1330.19, 1335.42, and 1365.16 MHz, respectively, which are very close to the experimental values of 1331.332687(20), 1336.68433(30), and 1366.84709(6) MHz. The calculated constants show deviations from experimental values by 0.1% for all the species, which gives confidence as to the accuracy of our calculations.

The  $B_0$  rotational constant calculated for HC<sub>5</sub>NH<sup>+</sup>, NC<sub>4</sub>NH<sup>+</sup>, and HC<sub>5</sub>O<sup>+</sup> were each scaled using the ratio  $B_{\text{expl}}/B_{\text{cal}}$  for HC<sub>5</sub>N, NC<sub>4</sub>N, and C<sub>5</sub>O, respectively. These values are shown in Table 2 together with the estimated values for the centrifugal distortion constant ( $D$ ), which were derived from the frequency calculations at CCSD/cc-pVTZ level of theory and scaled in the same manner as the rotational constants. The results of the same calculations at different levels of theory are given in Tables B.1 and B.2. Independent of the level of theory employed, our calculations provide a rotational constant value for HC<sub>5</sub>NH<sup>+</sup> around 1295.7 MHz, while that for NC<sub>4</sub>NH<sup>+</sup> is about 2.0 MHz lower, around 1293.6 MHz. In the case of HC<sub>5</sub>O<sup>+</sup>, the value is larger, around 1303.0 MHz. No large differences were found for the predicted values of the centrifugal distortion constants.

## 4. Discussion

The calculated rotational constants of HC<sub>5</sub>NH<sup>+</sup> and NC<sub>4</sub>NH<sup>+</sup> are very close to the value of  $B_0$  observed. A definitive assignment requires observations in the laboratory. Nevertheless, we could give some support to the assignment to HC<sub>5</sub>NH<sup>+</sup>. First, the ab initio calculations at all levels of theory predict a rotational constant for HC<sub>5</sub>NH<sup>+</sup> around 1295 MHz, while that of NC<sub>4</sub>NH<sup>+</sup> is systematically 2 MHz below. Second, the rota-

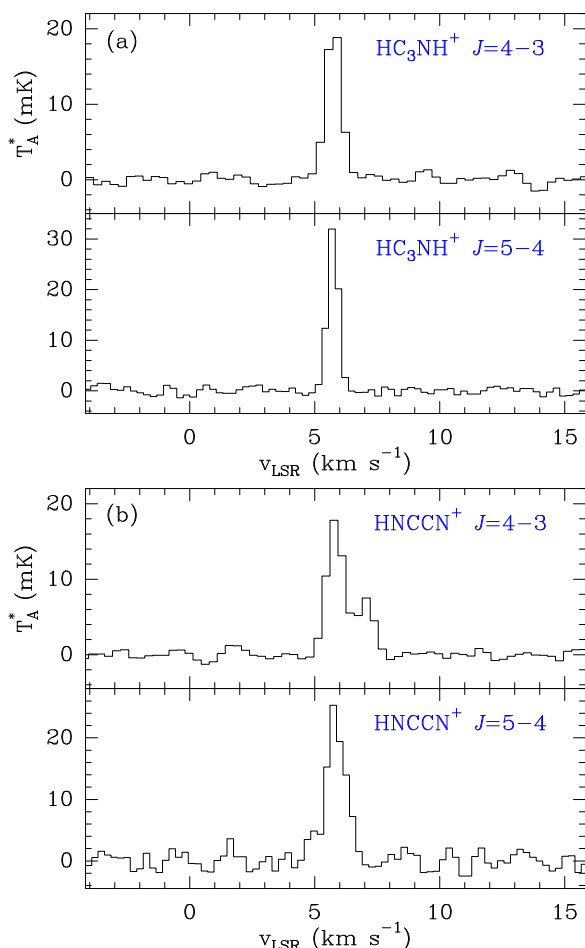


**Fig. 2.** Observed lines of  $\text{HC}_3\text{NH}^+$  (a) and of  $\text{HNCCN}^+$  (b). The abscissa corresponds to the local standard of rest velocity in  $\text{km s}^{-1}$ . Frequencies and intensities for the observed lines are given in Table 3. The ordinate is the antenna temperature corrected for atmospheric and telescope losses in mK. The  $J=4-3$  line of  $\text{HNCCN}^+$  shows two components due to the hyperfine structure introduced by the external nitrogen atom. Spectral resolution is 38.1 kHz.

tional constant corrected for the ratio theory-to-observation of the reference species,  $\text{HC}_5\text{N}$  and  $\text{NC}_4\text{N}$ , provide an excellent match with the observed  $B_0$  for protonated cyanodiacetylene within 0.05%, while the difference for protonated dicyanoacetylene reaches 0.2%.

Additional support for the assignment to  $\text{HC}_5\text{NH}^+$  comes from the comparison of the proton affinities of  $\text{HC}_5\text{N}$  and  $\text{NC}_4\text{N}$ . As previously indicated, the abundance of a protonated species depends on the abundance and proton affinity of the neutral counterpart. A large proton affinity permits the transfer of  $\text{H}^+$  to the neutral species,  $\text{M}$ , through the reactions  $\text{M} + \text{XH}^+ \rightarrow \text{MH}^+ + \text{X}$ , where  $\text{XH}^+$  is an abundant proton donor, such as  $\text{HCO}^+$  or  $\text{H}_3^+$ . For cyanodiacetylene,  $\text{HC}_5\text{N}$ , the proton affinity was measured to be  $770 \pm 20 \text{ kJ mol}^{-1}$  (Edwards et al. 2009). The abundance of this species is large in cold dark cores, hence, we could expect a moderately high abundance for its protonated form. Due to the lack of a permanent dipole, species such as  $\text{NCCN}$  and  $\text{NC}_4\text{N}$  have not been observed in dark clouds so far. Nevertheless, the detection of  $\text{NCCNH}^+$  in these objects by Agúndez et al. (2015) suggests that  $\text{NCCN}$  has an abundance as large as  $(1-10) \times 10^{-8}$  relative to  $\text{H}_2$ , that is to say it is similar to that of  $\text{HC}_3\text{N}$ . Assuming an abundance for  $\text{NC}_4\text{N}$  that is similar to that of  $\text{HC}_5\text{N}$ , then the relative abundances of  $\text{HC}_5\text{NH}^+$  and

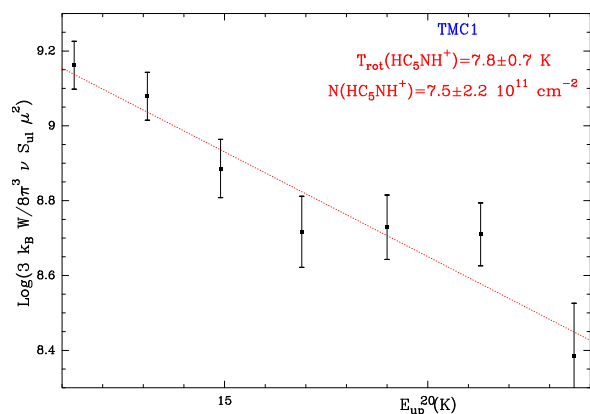


**Fig. 3.** Rotational diagram of the observed lines in TMC-1 assuming a dipole moment of 3.3 D, i.e. assuming the carrier of the lines is  $\text{HC}_5\text{NH}^+$ .

$\text{NC}_4\text{NH}^+$  depend on the proton affinities of the neutrals and on their electronic dissociative recombination rates, which in principle could be assumed to be similar. For  $\text{NC}_4\text{N}$ , there is not an experimental value in the literature, so we calculated it at CCSD/cc-pVTZ level of theory. We used the energy balance between  $\text{NC}_4\text{N} + \text{H}^+$  and  $\text{NC}_4\text{NH}^+$ , considering  $\text{NC}_4\text{N}$  and  $\text{H}^+$  are independent species. We found a proton affinity value for  $\text{NC}_4\text{N}$  of 736 kJ/mol. Using the same scheme, we obtained a proton affinity value for  $\text{HC}_5\text{N}$  of 783 kJ/mol, which is very close to the experimental one (see above). Hence, the proton affinity of  $\text{NC}_4\text{N}$  is lower than that of  $\text{HC}_5\text{N}$ , which favours the protonated form of  $\text{HC}_5\text{N}$  as a carrier of our lines.

Another argument supporting this assignment concerns the very different dipole moment of the two species. While,  $\text{HC}_5\text{NH}^+$  has a predicted dipole moment of  $\sim 3.3 \text{ D}$ , the corresponding value for  $\text{NC}_4\text{NH}^+$  is  $\sim 9.5 \text{ D}$  (see Table 2). Hence, the abundance resulting from the observed line intensities would be significantly different if the carrier were to be one versus the other species. In Fig. 3 we show the rotational diagram obtained from the observed intensities (see Table 1) assuming that the carrier is  $\text{HC}_5\text{NH}^+$ . We adopted a source radius of  $40''$  (Fossé et al. 2001). The parameter that is really interesting from this plot is the derived rotational temperature as the column density depends on the assumed dipole moment. The observed lines can be reproduced with a  $T_{\text{rot}}$  of  $7.8 \pm 0.7 \text{ K}$ . This is a typical value of the rotational temperature for most molecules detected so far in TMC-1, but that could require a very large  $\text{H}_2$  volume density if the dipole moment were 9.5 D, that is, if the carrier were  $\text{NC}_4\text{NH}^+$ . The derived column density is  $(7.5 \pm 2.2) \times 10^{11}$  if the carrier is  $\text{HC}_5\text{NH}^+$ , and  $\sim 9 \times 10^{10} \text{ cm}^{-2}$  if the carrier is  $\text{NC}_4\text{NH}^+$ .

Hence, we consider that we have arguments to support the assignment of the lines to protonated cyanodiacetylene. Cernicharo et al. (2020) performed a rotational analysis to all the transitions of  $\text{HC}_5\text{N}$  observed in our line survey. They derived  $T_{\text{rot}} = 8.6 \pm 0.2 \text{ K}$  and  $N(\text{HC}_5\text{N}) = (1.8 \pm 0.2) \times 10^{14} \text{ cm}^{-2}$ . This column density was derived from the observed weak hyperfine components in the  $\text{HC}_5\text{N}$  transitions from  $J=12-11$  up to  $J=16-15$  in order to take line opacity effects into account. Hence, we derived an abundance ratio of  $\sim 240$  for  $\text{HC}_5\text{N}/\text{HC}_5\text{NH}^+$ .

Another indirect indication supporting our identification could arise from the comparison of the abundances of other protonated species, in particular  $\text{HC}_3\text{NH}^+$  and  $\text{NCCNH}^+$ . Both species are present in TMC-1 (Kawaguchi et al. 1994; Agúndez et al. 2015) and two rotational lines of each one are within our line survey. Fig. 2 shows the observed

**Table 3.** Observed line parameters for HC<sub>3</sub>NH<sup>+</sup> and HNCCN<sup>+</sup>.

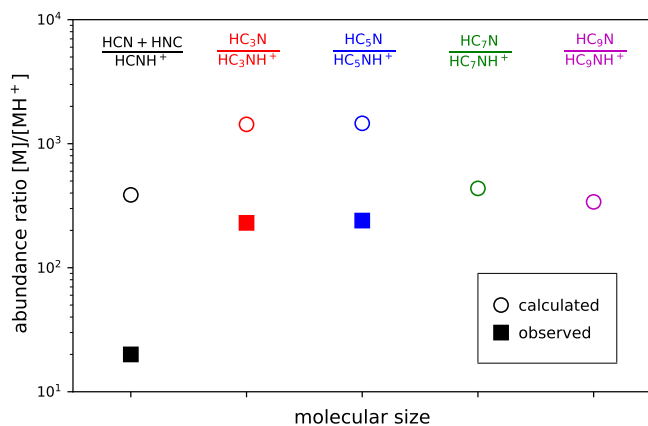
$J_u$	$\nu_{rest}^a$ (MHz)	$v_{LSR}$ (km s <sup>-1</sup> )	$\Delta v$ (km s <sup>-1</sup> )	$\int T_A^* dv$ (mK km s <sup>-1</sup> )	$T_A^*$ (mK)
HC <sub>3</sub> NH <sup>+</sup>					
4	34631.859	5.76±0.02	0.72±0.02	16.1±1	20.9
5	43289.740	5.74±0.02	0.52±0.01	18.1±1	32.7
HNCCN <sup>+</sup>					
4 <sup>b</sup>	35503.840	5.86±0.03	0.76±0.07	6.1±1	7.5
4 <sup>c</sup>	35503.981	5.82±0.01	0.82±0.03	15.7±1	18.0
5	44379.851	5.86±0.02	0.90±0.04	22.9±1	23.8

**Notes.**

(<sup>a</sup>) Rest frequencies. The uncertainty is typically 2-3 kHz.

(<sup>b</sup>) Corresponds to the  $F=3-2$  hyperfine component.

(<sup>c</sup>) Corresponds to the unresolved hyperfine components  $F=4-3$  &  $5-4$ .


**Fig. 4.** Abundance ratios between neutral and protonated species for the series of cyanopolynes. Calculated values correspond to a chemical model of a cold dark cloud at the steady state and observed ones to TMC-1.

lines of both species. The corresponding line parameters are given in Table 3. From the observed intensities, we derived  $N(\text{HC}_3\text{NH}^+) = 1.0 \times 10^{12} \text{ cm}^{-2}$  and  $N(\text{HNCCN}^+) = 9.0 \times 10^{10} \text{ cm}^{-2}$ , that is,  $N(\text{HC}_3\text{NH}^+)/N(\text{HNCCN}^+) \sim 14$ . Cernicharo et al. (2020) also derived a column density for HC<sub>3</sub>N of  $(2.3 \pm 0.2) \times 10^{14} \text{ cm}^{-2}$ , which was corrected for line opacity effects. Therefore, the derived abundance ratio for HC<sub>3</sub>N/HC<sub>3</sub>NH<sup>+</sup> is  $\approx 230$ , which is a value that is in good agreement with the one found by Kawaguchi et al. (1994)  $\sim 160$  and it is very similar to what was found above for HC<sub>5</sub>N/HC<sub>5</sub>NH<sup>+</sup>.

Between our unidentified features, we searched for lines that could be assigned to NC<sub>4</sub>NH<sup>+</sup> using our ab initio calculations without success. A search for lines of NCCCNC also provides an upper limit to its column density of  $\leq 10^{12} \text{ cm}^{-2}$ .

The case for HC<sub>5</sub>NH<sup>+</sup> is similar to that of the discovery of C<sub>3</sub>H<sup>+</sup> by Pety et al. (2012), which was done from the reasonable agreement between the observed rotational constant and the best ab initio calculations available at that moment for C<sub>3</sub>H<sup>+</sup>.

#### 4.1. Chemistry of protonated species

The chemistry of protonated molecules in cold dense clouds has been discussed by Agúndez et al. (2015). Here, we revisit the pseudo time-dependent gas-phase chemical model of a cold dark cloud carried out by these authors. The chemical network adopted is largely based on the UMIST RATE12 reaction net-

work (McElroy et al. 2013). For more details on the chemical model, we refer the reader to Agúndez et al. (2015). In cold dense clouds, protonated molecules MH<sup>+</sup> form mainly by the proton transfer from a proton donor XH<sup>+</sup> to M :



while they are destroyed through the dissociative recombination with electrons



Therefore, at the steady state, the neutral-to-protonated abundance ratio is

$$\frac{[\text{M}]}{[\text{MH}^+]} = \frac{k_{DR}}{k_{PT}} \frac{[\text{e}^-]}{[\text{XH}^+]}, \quad (3)$$

where  $k_{DR}$  and  $k_{PT}$  are the rate constants of the reactions of the dissociative recombination and proton transfer, respectively. The chemical model indicates that this scheme holds for HC<sub>3</sub>NH<sup>+</sup> and HC<sub>5</sub>NH<sup>+</sup>, where the main proton donor XH<sup>+</sup> is HCO<sup>+</sup>. Calculated neutral-to-protonated abundance ratios are about ten times higher than observed for HC<sub>3</sub>NH<sup>+</sup> and HC<sub>5</sub>NH<sup>+</sup> (see Fig. 4). That is to say, the chemical model underestimates the abundance of the protonated form with respect to its neutral counterpart. The rate constants of the dissociative recombination and proton transfer from HCO<sup>+</sup> used in the chemical model are just estimates for HC<sub>5</sub>NH<sup>+</sup>; although, in the case of HC<sub>3</sub>NH<sup>+</sup>, they are well known from experiments (Anicich 2003; Geppert et al. 2004). We note that the chemical model also underestimates the abundance of HCNH<sup>+</sup> (see Fig. 4) and other protonated species, such as HCS<sup>+</sup> and NH<sub>3</sub>, regardless of the cosmic-ray ionisation adopted (Agúndez et al. 2015). We suspect that the most likely reason for the underestimation of protonated molecules in the chemical model is the existence of additional formation routes that are not considered in the model.

*Acknowledgements.* The Spanish authors thank Ministerio de Ciencia e Innovación for funding support through project AYA2016-75066-C2-1-P. We also thank ERC for funding through grant ERC-2013-Syg-610256-NANOCOSMOS. MA thanks Ministerio de Ciencia e Innovación for Ramón y Cajal grant RyC-2014-16277.

## References

- Adler, T. B., Knizia, G., Werner, H.-J., 2007 J. Chem. Phys. 127, 221106  
 Agúndez, M. & Wakelam, V. 2013, Chem. Rev., 113, 8710  
 Agúndez, M., Cernicharo, J., de Vicente, P., et al., 2015, A&A, 579, L10  
 Agúndez, M., Marcelino, N., Cernicharo, J., 2018, ApJ, 861, L22  
 Alexander, A. J., Kroto, H. W., Walton, D. R. M., 1976, J. Mol. Spectrosc., 62, 175  
 Anicich, V. G. 2003, JPL Publication 03-19  
 Bacmann, A., García-García, E., & Faure, A. 2016, A&A, 588, L8  
 Bizzocchi, L., Degli Esposti, C., Botschwina, P., 2004, J. Mol. Spectrosc., 225, 145  
 Botschwina, P., Heyl, Ä., Oswald, R., Hirano, T., 1997, SActA, 53, 1079  
 Botschwina, P., Heyl, A., Chen, W., et al., 1998, J. Chem. Phys., 109, 3108  
 Cernicharo, J. 1985, Internal IRAM report (Granada: IRAM)  
 Cernicharo, J., 2012, in ECLA 2011: Proc. of the European Conference on Laboratory Astrophysics, EAS Publications Series, 2012, Ed.: C. Stehl, C. Joblin, & L. d'Hendecourt (Cambridge: Cambridge Univ. Press), 251; [https://nanocosmos.iff.csic.es/?page\\_id=1619](https://nanocosmos.iff.csic.es/?page_id=1619)  
 Cernicharo, J., Tercero, B., Fuente, A., et al. 2013, ApJ, 771, L10  
 Cernicharo, J., et al., 2020, A&A, submitted  
 Cížek, J., in "Advances in Chemical Physics" (P. C. Hariharan, Ed.), Vol.14, 35, Wiley Interscience, New York, 1969  
 Edwards, S.J., Freeman, C.G., McEwan, J., 2009, Int. J. Mass Spectrom., 279, 82  
 Fossé, D., Cernicharo, J., Gerin, M., Cox, P., 2001, ApJ, 552, 168

- Frisch, M. J., Trucks, G. W., Schlegel, H. B., et al. 2013, Gaussian 09, revision D.01
- Geppert, W. D., Ehlerding, A., Hellberg, F., et al. 2004, ApJ, 613, 1302
- Giesen, T.F., Harding, M.E., Gauss, J. et al., 2020, J. Mol. Spectrosc., 371, 111303
- Gordy, W., & Cook, R.L., 1984, Microwave Molecular Spectra, Chapter V, Wiley, New York.
- Gronowski, M., Kolos, R., 2006, J. Mol. Struct., 834, 102
- Hirahara, Y., Ohshima, Y., Endo, Y., 1994, J. Chem. Phys., 101, 7342
- Hill, J. G., Mazumder, S., Peterson, K. A., 2010a, J. Chem. Phys., 132, 054108
- Hill, J. G., Peterson, K. A., 2010b, Phys. Chem. Chem. Phys., 12, 10460
- Hunter, E. P. & Lias, S. G. 1998, J. Phys. Chem. Ref. Data, 27, 413
- Kawaguchi, K., Kasai, Y., Ishikawa, S. et al., 1994, ApJ, 420, L95
- Kaifu, N., Ohishi, M., Kawaguchi, K., et al., 2004, PASJ, 56, 69
- Knizia, G., Adler, T. B., Werner, H.-J., 2009 J. Chem. Phys. 130, 054104
- Lique, F., Cernicharo, J., Cox, P., 2006, ApJ, 653, 1342
- Marcelino, N., Agúndez, M., Cernicharo, J., et al. 2018, A&A, 612, L10
- McCarthy, M.C., Cooksy, A.L., Mohamed, S., et al., ApJS, 2003, 194, 287
- McElroy, D., Walsh, C., Markwick, A. J., et al. 2013, A&A, 550, A36
- McGuire, B.A., Burkhardt, A.M., Shingledecker, C.N., 2017, ApJ, 843, L28
- Mohamed, S., McCarthy, M.C., Cooksy, A.L., et al., 2005, J. Chem. Phys., 123, 234301
- Müller, H.S.P., Schlöder, F., Stutzki, J., Winnewisser, G., 2005, J. Mol. Struct., 742, 215
- Ogata, T., Ohshima, Y., Endo, Y., 1995, J. Am. Chem. Soc., 117, 3593
- Pardo, J. R., Cernicharo, J., Serabyn, E. 2001, IEEE Trans. Antennas and Propagation, 49, 12
- Pety, J., Gúzman, V., Roueff, E., et al., 2012, A&A, 548, A68
- Pritchard, B. P., Altarawy, D., Didier, B., et al. 2019, J. Chem. Inf. Model., 59, 4814
- Raghavachari, K., Trucks, G. W., Pople, J. A., Head-Gordon, M., 1989, Chem. Phys. Lett., 157, 479
- Sakai, N., Sakai, T., Aikawa, Y., Yamamoto, S. 2008, ApJ, 675, L89
- Schilke, P., Walmsley, C. M., Millar, T. J., Henkel, C. 1991, A&A, 247, 487
- Thaddeus, P., Guélin, M., Linke, R. A. 1981, ApJ, 246, L41
- Turner, B. E., Terzieva, R., Herbst, E. 1999, ApJ, 518, 699
- Werner, H.-J., Knowles, P. J., Knizia, G., et al., 2018, MOLPRO, version 2018.1.
- Winther, F., Schönhoff, M., LePrince, R., et al., 1992, J. Mol. Spectrosc., 152, 205
- Xue, C., Willis, E. R., Loomis, R. A., et al., 2020, ApJ, 900, L9



**Table A.1.** Frequencies, upper energy levels, Einstein coefficients, and line strengths of HC<sub>5</sub>NH<sup>+</sup> transitions.

$J_u - J_l$	$\nu$ (MHz)	$E_{up}$ (K)	$A_{ul}$ (s <sup>-1</sup> )	$S_{ul}$
1- 0	2591.632±0.001	0.1	7.177×10 <sup>-10</sup>	1
2- 1	5183.262±0.001	0.4	6.890×10 <sup>-09</sup>	2
3- 2	7774.892±0.002	0.7	2.492×10 <sup>-08</sup>	3
4- 3	10366.520±0.002	1.2	6.125×10 <sup>-08</sup>	4
5- 4	12958.144±0.002	1.9	1.223×10 <sup>-07</sup>	5
6- 5	15549.766±0.003	2.6	2.147×10 <sup>-07</sup>	6
7- 6	18141.384±0.003	3.5	3.447×10 <sup>-07</sup>	7
8- 7	20732.997±0.003	4.5	5.188×10 <sup>-07</sup>	8
9- 8	23324.605±0.003	5.6	7.435×10 <sup>-07</sup>	9
10- 9	25916.207±0.003	6.8	1.025×10 <sup>-06</sup>	10
11-10	28507.802±0.003	8.2	1.371×10 <sup>-06</sup>	11
12-11	31099.391±0.003	9.7	1.786×10 <sup>-06</sup>	12
13-12	33690.971±0.003	11.3	2.278×10 <sup>-06</sup>	13
14-13	36282.543±0.003	13.1	2.852×10 <sup>-06</sup>	14
15-14	38874.105±0.003	14.9	3.516×10 <sup>-06</sup>	15
16-15	41465.658±0.003	16.9	4.276×10 <sup>-06</sup>	16
17-16	44057.200±0.003	19.0	5.138×10 <sup>-06</sup>	17
18-17	46648.732±0.003	21.3	6.109×10 <sup>-06</sup>	18
19-18	49240.251±0.004	23.6	7.195×10 <sup>-06</sup>	19
20-19	51831.758±0.006	26.1	8.402×10 <sup>-06</sup>	20
21-20	54423.251±0.008	28.7	9.738×10 <sup>-06</sup>	21
22-21	57014.731±0.010	31.5	1.121×10 <sup>-05</sup>	22
23-22	59606.197±0.012	34.3	1.282×10 <sup>-05</sup>	23
24-23	62197.647±0.015	37.3	1.458×10 <sup>-05</sup>	24
25-24	64789.082±0.018	40.4	1.649×10 <sup>-05</sup>	25
26-25	67380.500±0.021	43.7	1.856×10 <sup>-05</sup>	26
27-26	69971.902±0.025	47.0	2.080×10 <sup>-05</sup>	27
28-27	72563.285±0.029	50.5	2.322×10 <sup>-05</sup>	28
29-28	75154.650±0.033	54.1	2.581×10 <sup>-05</sup>	29
30-29	77745.996±0.038	57.8	2.859×10 <sup>-05</sup>	30
31-30	80337.323±0.043	61.7	3.156×10 <sup>-05</sup>	31
32-31	82928.629±0.048	65.7	3.473×10 <sup>-05</sup>	32
33-32	85519.914±0.054	69.8	3.811×10 <sup>-05</sup>	33
34-33	88111.177±0.060	74.0	4.170×10 <sup>-05</sup>	34
35-34	90702.419±0.067	78.4	4.550×10 <sup>-05</sup>	35
36-35	93293.637±0.073	82.8	4.953×10 <sup>-05</sup>	36
37-36	95884.831±0.081	87.4	5.380×10 <sup>-05</sup>	37
38-37	98476.002±0.089	92.2	5.830×10 <sup>-05</sup>	38

## Appendix A: Frequencies, intensities, and energies of HC<sub>5</sub>NH<sup>+</sup> transitions

In order to facilitate the search of HC<sub>5</sub>NH<sup>+</sup> towards other sources, we provide the frequencies, uncertainties, line strengths, Einstein coefficients, and upper energy levels for all transitions of this species below 100 GHz in Table A.1. The degeneracies of the energy levels are  $2J+1$ . The rotational partition function for HC<sub>5</sub>NH<sup>+</sup> can be derived for a given temperature  $T$  from the standard expression  $Q_{rot}=kT/hB$  (Gordy & Cook 1984), to be  $Q_{rot}=16.087 \times T$ .

## Appendix B: Additional quantum chemical calculation data

All structure optimisation calculations reported in this work were performed using the closed-shell coupled cluster with singles and doubles (CCSD) (Čížek 1969) and perturbative triple excitations (CCSD(T), Raghavachari et al. 1989) with and without an explicitly correlated (F12) approximation (Adler et al. 2007; Knizia et al. 2009). For CCSD and CCSD(T) calculations, we used Dunning’s correlation consistent polarised valence (and valence-core) triple- $\zeta$  basis sets cc-pVTZ (cc-pCVTZ), which

were also augmented with diffuse functions (aug-cc-pVTZ, Pritchard et al. 2019). On the other hand, with the calculations at the CCSD(T)-F12 level, the Dunning’s correlation consistent basis sets with polarised core-valence correlation triple- $\zeta$  for explicitly correlated calculations (cc-pCVTZ-F12; Hill et al. 2010a,b) was used. In this latter case, all electrons (valence and core) are correlated. In order to achieve an estimate of the  $B_0$  rotational constant, vibration-rotation interaction constants were calculated using second-order perturbation theory at the MP2/cc-pVTZ level. All the calculations were carried out using the Molpro 2018.1 (Werner et al. 2018) and Gaussian 09 (Frisch et al. 2013) programme packages.

The molecular structure for all the linear isomers of HC<sub>5</sub>NH<sup>+</sup> and NC<sub>4</sub>NH<sup>+</sup> species were calculated using CCSD/cc-pVTZ level of theory. We did not considered asymmetric structures because the carrier of the observed lines is a linear molecule. The relative energies of all plausible isomers, as well as their rotational constants and dipole moments obtained at the CCSD/cc-pVTZ level, are summarised in Table B.3. In both cases (C<sub>5</sub>H<sub>2</sub>N<sup>+</sup> and C<sub>4</sub>HN<sub>2</sub><sup>+</sup>), the considered species HC<sub>5</sub>NH<sup>+</sup> and NC<sub>4</sub>NH<sup>+</sup> are the lowest energy isomers, respectively.

Vibrational calculations were also conducted in order to estimate the energies, the IR intensities, and the first order vibration-rotation coupling constant (Table B.4). From these values, we derived the rotational constants  $B_v$  for each vibrational state following the expression (Gordy & Cook 1984):

$$B_v = B_e - \sum_i \alpha_i (v_i + \frac{1}{2} d_i), \quad (\text{B.1})$$

where  $B_e$  is the rotational constant at the equilibrium position and  $\alpha_i$  represents the first order vibration-rotation coupling constants for each  $i$  vibrational mode. Keeping in mind that the rotational constant of the vibrational ground state ( $B_0$ ) is obtained when the  $\nu$  for every vibrational mode is equal to zero ( $B_0 = B_e - \sum_i \frac{1}{2} \alpha_i d_i$ ), equation B.1 can be also expressed as  $B_v = B_0 - \sum_i \alpha_i v_i$ .

The values for the rotational constants of the fundamental vibrations,  $B_v$ , of HC<sub>5</sub>NH<sup>+</sup> and HNC<sub>4</sub>N<sup>+</sup> were corrected by the scale factor for HC<sub>5</sub>N and NC<sub>4</sub>N, respectively, which were obtained as follows:  $B_0$ , the experimental value (Bizzocchi et al. 2004; Winther et al. 1992, respectively), was divided by the theoretical values (MP2/cc-pVTZ level of theory for  $B_v$  estimations). In the case of the  $B_0$  values reported in Table B.2, we initially calculated the theoretical ground state rotational constant  $B_0$  ( $B_0 = B_e - \sum_i \frac{1}{2} \alpha_i d_i$ ), using the  $B_e$  value of the corresponding level of theory and the vibration-rotation coupling constants ( $\alpha$ ) from the MP2/cc-pVTZ anharmonic calculations, and, finally, we corrected the  $B_0$  values using a scale factor of HC<sub>5</sub>N and NC<sub>4</sub>N at the corresponding ab initio level of calculation.

From the energies of the vibrational modes, which were obtained theoretically, we could also estimate the vibrational partition function for the HC<sub>5</sub>NH<sup>+</sup> and HNC<sub>4</sub>N<sup>+</sup> species. They were calculated using the expression (Gordy & Cook 1984):

$$Q_v = \prod_i (1 - e^{-(h\omega_i/KT)})^{-d_i}, \quad (\text{B.2})$$

where  $\omega_i$  and  $d_i$  represent the energy and the degeneracy of each  $i$  vibrational mode. These energies for the vibrational modes are taken from the results of the ab initio calculations evaluated at the MP2/cc-pVTZ level of theory, under the anharmonic correction.

**Table B.1.** Theoretical values for spectroscopic parameters of HC<sub>5</sub>NH<sup>+</sup>, NC<sub>4</sub>NH<sup>+</sup>, and HC<sub>5</sub>O<sup>+</sup> at different levels of theory.

	HC <sub>5</sub> NH <sup>+</sup>			NC <sub>4</sub> NH <sup>+</sup>			HC <sub>5</sub> O <sup>+</sup>		
	$B_0^a$ (MHz)	$D^b$ (MHz)	$\mu$ (D)	$B_0^c$ (MHz)	$D^d$ (MHz)	$\mu$ (D)	$B_0^e$ (MHz)	$D^f$ (MHz)	$\mu$ (D)
CCSD(T)-F12;core/CVTZ-F12	1295.51		3.26	1293.54		9.47	1303.1		3.13
CCSD(T)/aug-cc-pVTZ	1295.98		3.22	1293.95		9.46	1303.4		3.22
CCSD(T)/cc-pCVTZ	1295.78		3.83	1293.77		9.47	1303.1		2.22
CCSD(T)/cc-pVTZ	1295.77		3.82	1293.87		9.45	1309.1		2.23
CCSD/aug-cc-pVTZ	1295.93		3.82	1293.54		9.94	1297.9		2.78
CCSD/cc-pCVTZ	1295.73		3.53	1293.46		9.93	1298.5		1.63
CCSD/cc-pVTZ	1295.67	$26.3 \times 10^{-6}$	3.55	1293.50	$27.8 \times 10^{-6}$	9.91	1297.9	$31.2 \times 10^{-6}$	1.65
MP2/cc-pVTZ	1296.20	$26.1 \times 10^{-6}$	3.64	1293.41	$27.6 \times 10^{-6}$	9.13	1304.7	$30.7 \times 10^{-6}$	2.07

**Notes.** <sup>(a)</sup> Rotational constants were corrected with the vibration-rotation interaction estimated at the MP2/cc-pVTZ level of theory and by the scaling factors found for HC<sub>5</sub>N. <sup>(b)</sup> Centrifugal distortion constant values were corrected using the scaling factor found for those calculated for HC<sub>5</sub>N. <sup>(c)</sup> Rotational constants were corrected with the vibration-rotation interaction estimated at the MP2/cc-pVTZ level of theory and by the scaling factors found for NC<sub>4</sub>N. <sup>(d)</sup> Centrifugal distortion constant values were corrected using the scaling factor found for those values calculated for NC<sub>4</sub>N. <sup>(e)</sup> Rotational constants were corrected with the vibration-rotation interaction estimated at the MP2/cc-pVTZ level of theory and by the scaling factors found for C<sub>5</sub>O. <sup>(f)</sup> Centrifugal distortion constant values were corrected using the scaling factor found for those values calculated for C<sub>5</sub>O.

**Table B.2.** Comparison of the experimental and theoretical values for spectroscopic parameters of HC<sub>5</sub>N, NC<sub>4</sub>N, and C<sub>5</sub>O at different levels of theory.

	HC <sub>5</sub> N		
	$B_0^a$ (MHz)	$D^b$ (MHz)	$\mu$ (D)
Experimental	1331.332687(20)	$30.1090 (15) \times 10^{-6}$	4.33 <sup>c</sup>
CCSD(T)-F12;core/CVTZ-F12	1330.19		4.88
CCSD(T)/aug-cc-pVTZ	1317.27		4.90
CCSD(T)/cc-pCVTZ	1318.29		4.33
CCSD(T)/cc-pVTZ	1317.73		4.33
CCSD/aug-cc-pVTZ	1324.51		4.84
CCSD/cc-pCVTZ	1325.30		4.32
CCSD/cc-pVTZ	1324.75	$27.0 \times 10^{-6}$	4.32
MP2/cc-pVTZ	1320.44	$26.8 \times 10^{-6}$	4.35
	NC <sub>4</sub> N <sup>d</sup>		
	$B_0^a$ (MHz)	$D^b$ (MHz)	
Experimental	1336.68433(30)	$31.44 (12) \times 10^{-6}$	
CCSD(T)-F12;core/CVTZ-F12	1330.13		
CCSD(T)/aug-cc-pVTZ	1322.36		
CCSD(T)/cc-pCVTZ	1323.40		
CCSD(T)/cc-pVTZ	1322.90		
CCSD/aug-cc-pVTZ	1330.13		
CCSD/cc-pCVTZ	1330.86		
CCSD/cc-pVTZ	1330.46	$28.3 \times 10^{-6}$	
MP2/cc-pVTZ	1323.60	$28.1 \times 10^{-6}$	
	C <sub>5</sub> O		
	$B_0^a$ (MHz)	$D^b$ (MHz)	$\mu$ (D)
Experimental	1366.84709(6)	$35.05 (51) \times 10^{-6}$	
CCSD(T)-F12;core/CVTZ-F12	1365.56		3.04
CCSD(T)/aug-cc-pVTZ	1350.44		2.92
CCSD(T)/cc-pCVTZ	1351.38		4.01
CCSD(T)/cc-pVTZ	1349.51		3.99
CCSD/aug-cc-pVTZ	1365.85		4.34
CCSD/cc-pCVTZ	1366.78		4.38
CCSD/cc-pVTZ	1365.27	$26.4 \times 10^{-6}$	4.36
MP2/cc-pVTZ	1350.69	$25.9 \times 10^{-6}$	4.49

**Notes.** <sup>(a)</sup> Rotational constants were corrected with the vibration-rotation interaction estimated at the MP2/cc-pVTZ level of theory (see text of section B). <sup>(b)</sup> Centrifugal distortion constant was only calculated at CCSD/cc-pVTZ and MP2/cc-pVTZ levels of theory. <sup>(c)</sup> Alexander et al. (1976). <sup>(d)</sup> NC<sub>4</sub>N is a non-polar species.



**Table B.3.** Relative energies, rotational constants, and electric dipole moments for HC<sub>5</sub>NH<sup>+</sup> and NC<sub>4</sub>NH<sup>+</sup> and all their isomers calculated at the CCSD/cc-pVTZ level of theory.

Isomer	$\Delta E$ (kcal/mol)	$B_e$ (MHz)	$\mu$ (D)
<b>C<sub>5</sub>H<sub>2</sub>N<sup>+</sup></b>			
HCCCCCNH <sup>+</sup>	0	1288.24	4.33
HCCCNCCCH <sup>+</sup>	18.47	1385.97	1.22
HCCCCCNCH <sup>+</sup>	20.99	1342.20	5.98
<b>C<sub>4</sub>HN<sub>2</sub><sup>+</sup></b>			
HNCCCCN <sup>+</sup>	0	1286.43	9.91
HNCCNC <sup>+</sup>	18.44	1363.81	7.87
HCCNCCN <sup>+</sup>	21.03	1392.43	6.50
HCCNCCN <sup>+</sup>	25.67	1387.78	4.36
HCCCCNN <sup>+</sup>	37.08	1357.83	0.15
HNCNCCC <sup>+</sup>	64.66	1423.10	6.90
HCCCNNC <sup>+</sup>	64.76	1457.42	4.72
HNCCNCC <sup>+</sup>	94.42	1408.11	8.86
HCNNCCC <sup>+</sup>	115.32	1479.97	9.38
HNNCCCC <sup>+</sup>	140.49	1382.25	6.48
HCCNCC <sup>+</sup>	145.28	1512.05	4.01

**Table B.4.** Rotational constants, energies, and IR Intensities for the vibrational modes of HC<sub>5</sub>NH<sup>+</sup> and HNC<sub>4</sub>N<sup>+</sup>.

Mode	HC <sub>5</sub> NH <sup>+</sup> <sup>(a)</sup>					HNC <sub>4</sub> N <sup>+</sup> <sup>(a)</sup>				
	E <sub>v</sub> <sup>(b)</sup>	I <sub>IR</sub> <sup>(c)</sup>	α <sub>v</sub> <sup>(d)</sup>	B <sub>v</sub> <sup>(e)</sup>	q <sub>v</sub> <sup>(f)</sup>	E <sub>v</sub> <sup>(b)</sup>	I <sub>IR</sub> <sup>(c)</sup>	α <sub>v</sub> <sup>(d)</sup>	B <sub>v</sub> <sup>(e)</sup>	q <sub>v</sub> <sup>(f)</sup>
ν <sub>1</sub>	3694	1382.293	1.048	1295.142		3491	1260.325	1.044	1293.961	
ν <sub>2</sub>	3428	140.639	0.881	1295.310		2240	513.091	3.812	1291.164	
ν <sub>3</sub>	2295	1057.223	3.898	1292.267		2130	363.857	4.319	1290.651	
ν <sub>4</sub>	2182	659.964	4.183	1291.981		1992	52.358	2.924	1292.061	
ν <sub>5</sub>	2021	60.844	2.546	1293.631		1194	26.120	2.879	1292.107	
ν <sub>6</sub>	1236	7.209	2.597	1293.580		608	23.291	1.041	1293.964	
ν <sub>7</sub>	630	30.504	0.963	1295.228		523	63.591	-1.082	1296.109	0.2652
ν <sub>8</sub>	711	32.967	-0.160	1296.361	0.1826	502	28.043	-1.414	1296.444	0.2750
ν <sub>9</sub>	529	15.163	-1.594	1297.807	0.2725	502	44.205	-1.103	1296.130	0.2652
ν <sub>10</sub>	509	9.260	-1.295	1297.505	0.2786	241	10.300	-2.579	1297.622	0.4563
ν <sub>11</sub>	408	122.178	-0.796	1297.002	0.2859	96	0.431	-2.888	1297.934	1.1186
ν <sub>12</sub>	254	0.168	-2.366	1298.585	0.4631					
ν <sub>13</sub>	99	11.423	-2.877	1299.101	1.1384					

**Notes.**

<sup>(a)</sup> Results of ab initio calculations evaluated under anharmonic correction at the MP2/cc-pVTZ level of theory.

<sup>(b)</sup> Energy of the corresponding ν vibrational mode in cm<sup>-1</sup>.

<sup>(c)</sup> Infrared intensity in units of km mol<sup>-1</sup>.

<sup>(d)</sup> Vibration-rotation coupling constants α estimated for each ν vibrational mode.

<sup>(e)</sup> Rotational constant B of the vibrational state ν estimated using the α values and corrected with the corresponding experimental B<sub>0</sub> (see text).

<sup>(f)</sup> l-doubling constant q<sub>v</sub><sup>e</sup> of the vibrational mode ν.

**Table B.5.** Vibrational partition function for HC<sub>5</sub>NH<sup>+</sup> and HNC<sub>4</sub>N<sup>+</sup> species.

Temperature (K)	HC <sub>5</sub> NH <sup>+</sup>	HNC <sub>4</sub> N <sup>+</sup>
300	30.61	28.61
100	1.85	1.91
80	1.48	1.52
60	1.22	1.24
50	1.13	1.14
45	1.09	1.10
40	1.06	1.07
35	1.04	1.04
30	1.02	1.02
25	1.01	1.01
20	1.00	1.00
15	1.00	1.00
10	1.00	1.00